Journal of Alloys and Compounds, 203 (1994) 235–241
JALCOM 897

Electrochemical and surface properties of $Zr(V_xNi_{1-x})_2$ alloys as hydrogen-absorbing electrodes in alkaline electrolyte

Andreas Züttel, Felix Meli and Louis Schlapbach
Institute of Physics, University of Fribourg, CH-1700 Fribourg (Switzerland)

(Received July 4, 1993)

Abstract

Multicomponent Zr–Ni-based alloys of the nominal composition $ZrNi_2$ have some promising properties as electrode materials in reversible metal hydride batteries.

We have prepared a series of pseudobinary $Zr(V_xNi_{1-x})_2$ alloys in small samples of 6 g by levitation melting. Their bulk properties were then characterized by means of X-ray diffraction, hydrogen storage capacity and plateau pressure measurements. The kinetics were studied by means of high rate dischargeability and exchange current densities. The cycle life of pressed powder electrodes was tested with two different compacting materials, copper and nickel. The surface composition of the alloy grains was analysed by means of X-ray photoelectron spectroscopy (XPS) before introduction into the electrolyte, after activation and in the corroded state.

For alloys of the cubic C15 (Cu_2Mg) structure the lattice parameter a depends linearly on the vanadium content. The hydrogen storage capacity reaches a maximum of about 350 mA h g^{-1} at the composition $Zr(V_{0.25}Ni_{0.75})_2$. Also, the stability of the hydrides depends strongly on the vanadium content, the room temperature plateau pressure rising to about 0.5 bar for $Zr(V_{0.15}Ni_{0.85})_2$. It does not follow the behaviour expected from the relative hydrogen affinities of the pure components (Zr > V > Ni). Changes in the crystal and/or electronic structure seem to be the reason. Under high rate discharge (120 mA g^{-1}) we have found that alloys of the composition $Zr(V_xNi_{1-x})_2$ with $0.1 \leqslant x \leqslant 0.25$ retain about 80% of their capacity. One factor affecting the rate of the discharge reaction is the charge transfer, which is measured by the exchange current density. The exchange current density is highest for $Zr(V_{0.2}Ni_{0.8})_2$. Values of 80 and 40 mA g^{-1} were determined for nickel- and copper-compacted electrodes respectively. Furthermore, nickel-compacted electrodes activate faster. However, they also corrode faster owing to the instability of nickel in the applied potential range. XPS analysis showed that activation of an electrode in an electrolyte causes the dissolution of oxides of vanadium from the surface layers and therefore an enrichment of nickel. The degradation process might involve oxidation of all the alloy elements, dissolution of the soluble oxides and/or loss of grain contact by the formation of electrically non-conducting oxides.

1. Introduction

In the last decade the development of metal hydride electrodes for rechargeable batteries has been very successful. Two types of alloys, the AB_5 ($LaNi_5$) and AB_2 ($ZrNi_2$) intermetallic compounds, demonstrate reasonably high capacities and good cyclic stability as electrode materials. The bulk composition of the alloy determines its capacity and the plateau pressure, *i.e.* the potential of the electrode, while the current densities, activation and corrosion are dependent on the composition of the surface layer.

Petkov *et al.* [1] made a careful study of Zr–Ni alloys in the $ZrNi_2$ composition range (from 64.8 to 69 at.% Zr). The X-ray diffraction pattern of the so-called λ_2 phase of $ZrNi_2$ corresponds to an f.c.c. lattice (space group $Fd3m$–O_h^7) with lattice parameter $a = 6.925 \pm 0.005$ Å. From calculated and experimental intensities they found the λ_2 phase to be of the $MgCu_2$ type, with Zr in 8(a) and Ni in 16(d) sites. The $ZrNi_2$ compound is formed by a peritectic transformation at 1190 °C. Sawa and Wakao [2] examined a series of $Zr(V_xNi_{1-x})_2$ alloys ($0.1 \leqslant x \leqslant 1$) and found $ZrV_{0.66}Ni_{1.34}$ to be a single phase of f.c.c.-type structure ($a = 7.102$ Å) with a density of 7.51 g cm^{-3}. The lattice expansion was determined as 1.3×10^{-6} m^3 mol_H^{-1} ($\Delta V/V = 14.4\%$ for H/M = 1). Thermodynamically $ZrV_{0.66}Ni_{1.34}$ was found to have $\Delta H = -29.2$ kJ mol_H^{-1} and $\Delta S = -72.1$ J mol_H^{-1} K^{-1}. The partial molar enthalpy ΔH_0 can be expressed in terms of the unit cell volume as $-\Delta H$ (kJ mol_H^{-1}) $= -150 + 0.5V$ (Å^3) (where V stands for the unit cell volume $V = a^3$). The overstoichiometric alloys $ZrV_{0.8}Ni_{1.2}Mn_{0.4}$ and $Ti_{0.8}Zr_{0.2}Ni_{0.75}$ were shown to have high electrochemical capacities (about 366 mA h g^{-1}) [3, 4]. Sawa *et al.* [5] studied the influence of oxidation treatment on Ti–Zr–Ni hydride electrodes and found that the cathodic current density depends strongly on the Zr content of the alloy.

SSDI 0925-8388(93)00897-8

In this paper we present the results of cycle life experiments and surface analysis of a series of $Zr(V_xNi_{1-x})_2$ alloys in the composition range of $0 \leqslant x \leqslant 0.4$. This range appears to be most interesting from the point of view of capacities and good kinetics. We present our results in three parts. The first part deals with bulk properties such as structure, capacity and plateau pressure. The second part concerns the kinetics, *e.g.* high rate dischargeability and exchange current density, and the cycle life properties of the electrode. In the third part we present the results of surface analysis which will serve to explain the mechanisms of activation and degradation.

2. Experimental details

The $Zr(V_xNi_{1-x})_2$ ($0 \leqslant x \leqslant 0.4$) alloy samples were prepared by r.f. levitation melting in a water-cooled copper levitation crucible under a vacuum of 10^{-6} mbar. Appropriate quantities of the elements were used to produce a 6 g sample (Zr 99.8% from Goodfellow, V 99.7% from Koch–Light and Ni 99.99% from Johnson–Matthey). After melting for 5 min at 1300 °C the pellet was quenched to room temperature. The sample was crushed, then analysed by Debye–Scherrer X-ray diffraction. A portion of 2 g of the alloy was powdered using hydrogen gas at 40 bar and room temperature. The alloy hydrided within the first 10 min and disintegrated into a powder.

For the electrochemical measurements approximately 25 mg of the alloy powder were mixed with copper powder (Merck p.a., less than 63 μm) or nickel powder (Merck p.a., less than 10 μm) in a weight ratio of 1:3 and cold pressed (500 MPa) to a pellet ($d = 7$ mm). Copper-free pellets were prepared for X-ray photoelectron spectroscopy (XPS) analysis by introducing the powder into a high void nickel foam and then pressing it in air at room temperature. The electrodes were charged and discharged electrochemically in a 6 M KOH electrolyte. The discharge cut-off potential was −0.6 V referenced to the $Hg/HgO/OH^-$ electrode. The electrodes were tested in a half-cell experiment using constant charge (5 mA) and discharge (2.5 mA) currents. An additional discharge at one-tenth of the normal discharge current was carried out every 10 cycles. The exchange current densities were measured using half-charged electrodes and the equilibrium characteristics of the electrodes were measured using special cycles of pulsed charging and discharging (8 mA h g^{-1} per pulse).

For the surface analysis the samples were rinsed from KOH in doubly distilled water and dried in air at room temperature. They were then introduced into the ultrahigh vacuum of the spectrometer (less than 10^{-10} mbar base pressure, 10^{-9} mbar H_2 partial pressure after introducing the degassing sample). The surface concentrations were measured by means of X-ray photoelectron spectroscopy in a VG Escalab 5 spectrometer using Mg Kα radiation of energy 1253.6 eV (Au $4f_{7/2}$ at 84.0 eV, 1.7 eV full width at half-maximum (FWHM)). The measured surface composition is actually an average over an area of 0.2 cm^2 and to a depth of 10–20 Å. The sputter depth profiles (Ar^+, 2 keV) were evaluated using a standard sputtering rate of 500 Å cm^2 min^{-1} mA^{-1} (4 Å min^{-1}). They are therefore only precise to within a factor of 2.

3. Results

3.1. X-Ray diffraction

The alloys were analysed after melting and after a few charge–discharge cycles in hydrogen gas. Figure 1 shows the calculated lattice parameter a for the cubic C15 structure as a function of the vanadium content. In the $Zr(V_xNi_{1-x})_2$ composition range $0.15 \leqslant x \leqslant 0.4$ the lattice parameter increases linearly with vanadium content according to the relation a (Å) $= 6.915 + 0.448$ x. For the alloys with $x < 0.15$ we found a lattice parameter smaller than that given by the linear relation. The alloy of nominal composition $ZrNi_2$ was a multiphase alloy. The lattice parameter after a few hydrogen gas cycles was enlarged differently. This difference was minimal for $ZrV_{0.3}Ni_{1.7}$ owing to there being less residual hydrogen in the alloy as a result of the high plateau pressure.

3.2. Discharge capacities

Figure 2 shows the discharge capacity of the $Zr(V_xNi_{1-x})_2$ alloys as a function of the vanadium content using copper- and nickel-compacted electrodes.

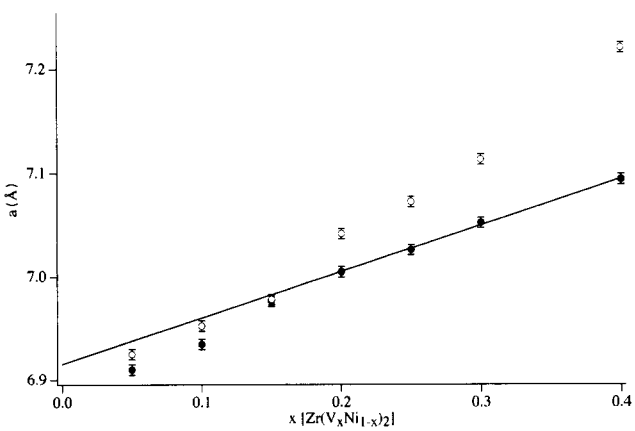

Fig. 1. Lattice parameter a for the cubic C15 structure of $Zr(V_xNi_{1-x})_2$ alloys as a function of vanadium content x: freshly prepared and mechanically pulverized alloy (●) and after a few hydrogen gas charge–discharge cycles (○).

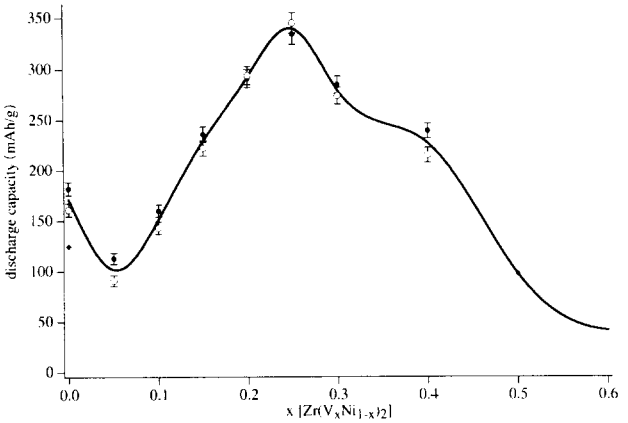

Fig. 2. Discharge capacity of $Zr(V_xNi_{1-x})_2$ alloy electrodes as a function of vanadium content. The discharge current was 12 mA h g^{-1}. Electrodes were compacted in a matrix of copper powder (●) or nickel powder (○). Values obtained by Sawa and Wakao [2] are also included (◆).

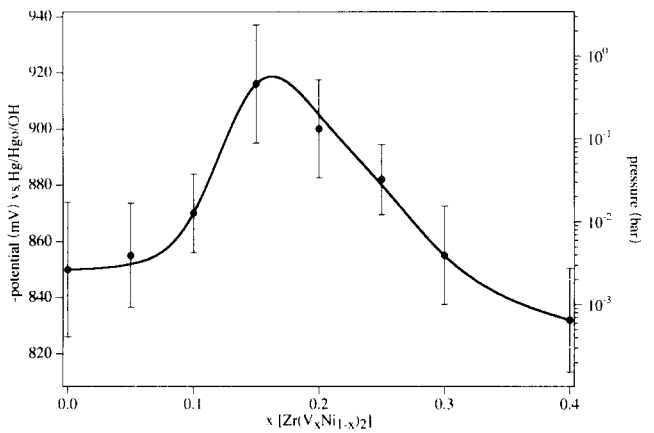

Fig. 3. Plateau potential of $Zr(V_xNi_{1-x})_2$ alloys as a function of vanadium content x. Bars represent the length of the plateau, *i.e.* the FWHM of the density-of-states distribution of hydrogen in interstitial sites.

An additional low discharge current of about 12 mA g^{-1} was used. The capacities measured by Sawa and Wakao [2] at a discharge current of about 17 mA g^{-1} are also included in the figure. The maximum discharge capacity was found for $ZrV_{0.5}Ni_{1.5}$; it reaches the very interesting value of 350 mA h g^{-1}. No significant difference between the nickel- and copper-compacted electrodes was found.

3.3. Equilibrium potential

From the measured equilibrium potential during pulsed discharge cycles we have calculated the potential for the maximum density of states for hydrogen in the interstitial sites using the method of Jaggy *et al.* [6]. Figure 3 shows the calculated potential and the corresponding plateau pressure for the $Zr(V_xNi_{1-x})_2$ alloys as a function of the vanadium content. The plateau pressure was calculated using a previously published method [7] from the Nernst equation for the hydrogen reference electrode. The error bars represent the FWHM of the energy distribution (*i.e.* pressure distribution). For the $ZrV_{0.3}Ni_{1.7}$ alloy we found a maximum plateau pressure of 0.5 bar at room temperature.

3.4. High rate dischargeability

Two different methods were used for measuring the kinetics of the electrodes. First the discharge capacity at high current (about 120 mA g^{-1}) is compared with the discharge capacity at low current (about 12 mA g^{-1}). Figure 4 shows the high current capacity as a percentage of the low current capacity as a function of the vanadium content. The capacity is about 80% of the capacity at low current after high current discharge for $Zr(V_xNi_{1-x})_2$ alloys with $0.15 \leqslant x \leqslant 0.3$. The second method consists of the measurement of the exchange current density as a function of the vanadium content, the results of which are shown in Fig. 5. The copper-

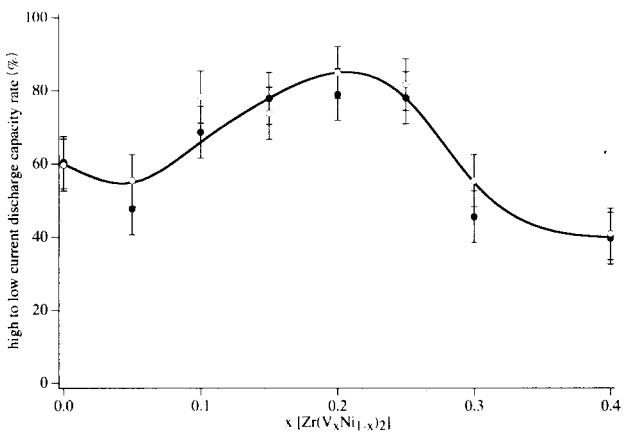

Fig. 4. Discharge capacity at high current rate (120 mA h g^{-1}) as a percentage of discharge capacity at low current rate (12 mA h g^{-1}). Electrodes were compacted in a copper powder matrix (●) or nickel powder matrix (○).

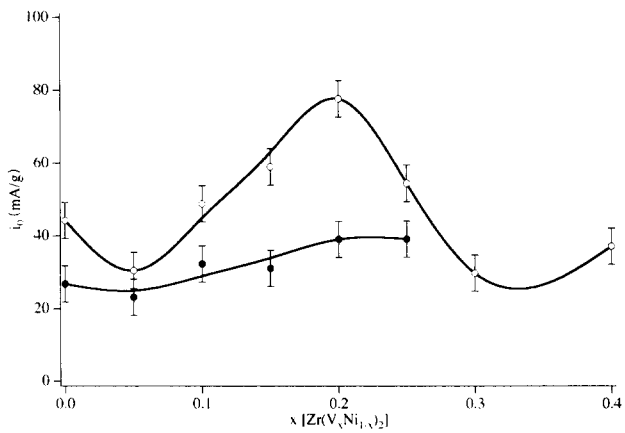

Fig. 5. Exchange current density i_0 as a function of vanadium content x for $Zr(V_xNi_{1-x})_2$ alloys. Electrodes were compacted in a copper powder matrix (●) or nickel powder matrix (○).

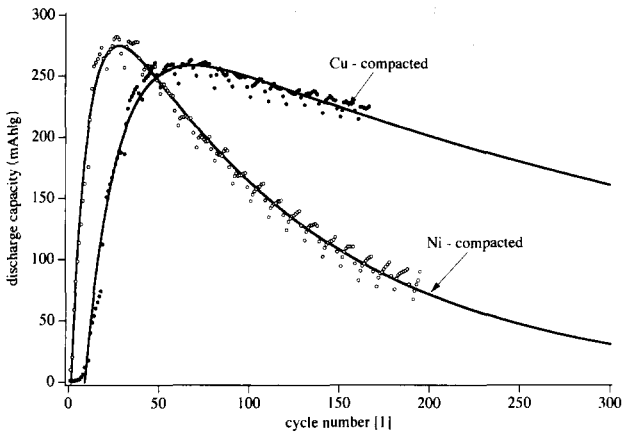

Fig. 6. Cycle life curves for nickel- and copper-compacted $ZrV_{0.5}Ni_{1.5}$ as a function of cycle number at discharge currents of 107 and 118 mA g^{-1} respectively.

and nickel-compacted electrodes showed surprisingly different behaviours: whereas the exchange current density of copper-compacted electrodes rises smoothly from 25 to 40 mA g^{-1} as a function of the vanadium content, that of nickel-compacted electrodes exhibits a pronounced maximum of about 80 mA g^{-1} for the $ZrV_{0.4}Ni_{1.6}$ alloy.

3.5. Cycle life

We observed a large difference between the copper- and nickel-compacted electrodes in terms of the development of the discharge capacity as a function of the cycle number. Figure 6 shows the cycle life curves for the $ZrV_{0.5}Ni_{1.5}$ alloy. While the copper-compacted alloy needed about 70 cycles to reach maximal capacity, the nickel-compacted electrodes needed only 30 cycles and had a higher maximum capacity. The cycle life parameters were calculated using a previously published model [8]. From this fit of the cycle life curve the resulting capacities, activation and oxidation constants were determined and are summarized in Table 1.

3.6. Potential after charge and discharge

The potential remaining after charge and discharge indicates the depth of charge and discharge respectively. Figure 7 shows these potentials as a function of the

TABLE 1. Total capacity (C_{tot}), active start-up capacity (C_a^0), activation (λ_{act}) and degradation (λ_{ox}) constants and maximum measured capacity (Max. cap.) for various ZrV_xNi_{1-x} alloys

Alloy	Compacting material	Current (mA g^{-1})	C_{tot} (mA h g^{-1})	C_a^0 (mA h g^{-1})	λ_{act} (% $cycle^{-1}$)	λ_{ox} (% $cycle^{-1}$)	Max. cap.
$ZrNi_2$	Cu	70.7	160	88	0.416	−0.0353	110
	Cu	7.1	204	166	0.683	0.00382	182
	Ni	120.0	95	85	0.0181	−0.174	114
	Ni	12.0	154	27	97.4	−0.0591	171
$ZrV_{0.1}Ni_{1.9}$	Cu	75.2	83	28	0.767	−0.0727	54
	Cu	7.5	140	100	0.484	−0.00107	113
	Ni	114.7	42	2	15.62	−0.170	60
	Ni	11.5	88	−63	94.8	−0.0395	96
$ZrV_{0.2}Ni_{1.8}$	Cu	75.2	103	62	5.58	−0.095	110
	Cu	7.5	173	147	1.87	0.040	160
	Ni	116.3	110	39	8.58	−0.047	112
	Ni	11.6	142	−1.5	36.95	−0.0169	143
$ZrV_{0.3}Ni_{1.7}$	Cu	61.3	177	48	11.1	−0.051	184
	Cu	6.1	256	217	3.20	0.095	236
	Ni	114.2	163	12	24	0.079	164
	Ni	11.4	225	−163	65	0.100	222
$ZrV_{0.4}Ni_{1.6}$	Cu	452.0	228	−13	1.93	0.0069	227
	Ni	133.7	269	1	11.0	0.21	250
	Ni	13.3	304	120	20.9	0.15	294
$ZrV_{0.5}Ni_{1.5}$	Cu	409.1	147	−14	1.61	−0.0225	168
	Ni	106.8	366	24	9.11	1.01	282
	Ni	10.7	419	280	8.41	0.74	345
$ZrV_{0.6}Ni_{1.4}$	Cu	223.2	80	−1.0	1.92	−0.0127	88
	Ni	128.2	181	11	2.17	0.13	152
	Ni	12.8	284	20	8.75	0.052	274
$ZrV_{0.8}Ni_{1.2}$	Cu	328.5	81	−10	1.92	−0.0012	83
	Ni	105.5	91	10	6.53	0.098	88
	Ni	10.6	244	56	6.03	0.236	215

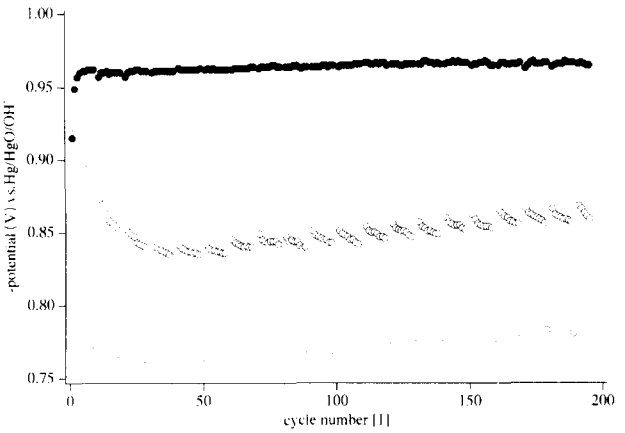

Fig. 7. Potential after charging (●), after high rate discharging (107 mA g^{-1}) and after low rate discharging (11 mA g^{-1}) (○) for nickel-compacted $ZrV_{0.5}Ni_{1.5}$ as a function of cycle number.

cycle number for the nickel-compacted $ZrV_{0.5}Ni_{1.5}$ alloy electrode. The potential remaining after charging increased within the first 5 cycles to a maximum of −0.962 V (referenced to the $Hg/HgO/OH^-$ electrode). It then remained constant over further cycles. The potential remaining after discharging decreased within the first 40 cycles to −0.830 V (referenced to the $Hg/HgO/OH^-$ electrode) for the high rate discharge of 120 mA g^{-1} and to −0.760 V for the low rate discharge. After 40 cycles both potentials increased slightly again.

3.7. XPS depth profile

The surface composition of $ZrV_{0.4}Ni_{1.6}$ alloy electrodes was analysed (a) before introducing them into the electrolyte, (b) after 30 electrochemical activation cycles and finally (c) after 300 electrochemical cycles. The core levels Zr $3d_{5/2}$ (180 eV), V $2p_{3/2}$ (513 eV) and Ni $2p_{3/2}$ (855 eV) were measured to evaluate the concentration and oxidation state of the components as a function of depth (to 400 Å). The results are shown in Figs. 8(a), 8(b) and 8(c) for Zr, V and Ni respectively. Most of the surface zirconium was oxidized. The zirconium composition did not change markedly upon activation of the electrode. At a depth of 30 Å the total amount of zirconium (metallic and oxidized) was approximately 1 atom/AB_2 in both cases. After 300 cycles the zirconium was only slightly more oxidized. Vanadium was fully oxidized in the top surface layer before activation. The activated sample did not have vanadium in the top layer, but in both samples the vanadium content increased to 0.3 atom/AB_2 at 30 Å. After 300 cycles there was no evidence of vanadium to a depth of 40 Å. Nickel was enriched in the top layers during cycling from 0.2 atom/AB_2 before activation to 1 atom/AB_2 in the activated sample and more than 2 atoms/AB_2 after 300 cycles. At a depth of 40 Å the nickel concentration was about 1.5 atoms/AB_2 in all samples and remained constant throughout the measured depth.

4. Discussion

We have studied $Zr(V_xNi_{1-x})_2$ alloys in the compositional range $0 \leqslant x \leqslant 0.4$. For $x > 0.1$ the alloys crystallized with a cubic C15 structure. The lattice parameter a showed a linear dependence on the vanadium content. This is in good agreement with the size of the atoms (V > Ni) and the ideal assumption that vanadium occupies nickel sites. The lattice parameter after a few hydrogen gas cycles was slightly larger than that of the virgin alloy. This can be explained by some hydrogen remaining in the alloy after dehydrogenation owing to the low plateau pressure. The electrochemical discharge capacity at low current is a good measure of the number of interstitial sites available to H. With increasing vanadium content the number of most favourable tetrahedral sites Zr_2V_2 and $Zr_2V_1Ni_1$ increases [2]. However, with increasing vanadium content the plateau pressure decreases and the concentration of the electrochemically most active element for the discharge reaction, nickel, decreases. This means that the overpotential during discharge increases with increasing vanadium content. Summing these opposite effects gave the maximum capacity for $ZrV_{0.5}Ni_{1.5}$. Furthermore, the maximum electrochemical capacity proved to be independent of the matrix powder(copper or nickel). As was mentioned, the lattice parameter values of the $Zr(V_xNi_{1-x})_2$ alloys with low vanadium contents ($x \leqslant 0.1$) were too small compared with the linear extrapolation from the other alloys. The plateau pressure and correspondingly the electrochemical equilibrium potential decreased with increasing vanadium content for all except the alloys with $x \leqslant 0.1$. Their plateau pressures were lower than that of $ZrV_{0.3}Ni_{1.7}$, which had the maximum plateau pressure. The reason for this is the increasing binding energy (vanadium has a higher chemical affinity for hydrogen than nickel does) for hydrogen and the increasing lattice parameter with increasing vanadium content. For the alloys with $x \leqslant 0.1$ there is no simple explanation for the low plateau pressure, though possibly a change in the crystal and/or electronic structure influences the absorption enthalpy.

Comparison of the discharge capacities at low and high currents gives a measure of the kinetics of the electrode [9]. We observed about 80% of the maximum capacity for alloys with $0.1 < x < 0.3$. Higher and lower vanadium contents result in smaller quotas. If hydrogen absorption–desorption in the electrolyte is considered to be a heterogeneously catalysed reaction, we may divide the whole process during discharge into a sequence of elementary steps. These steps consist of (1)

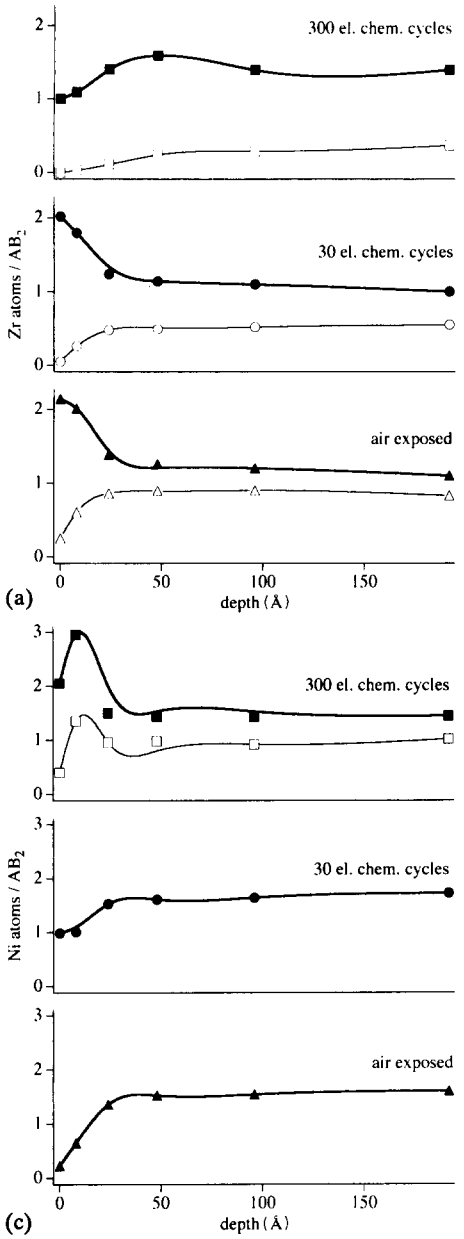

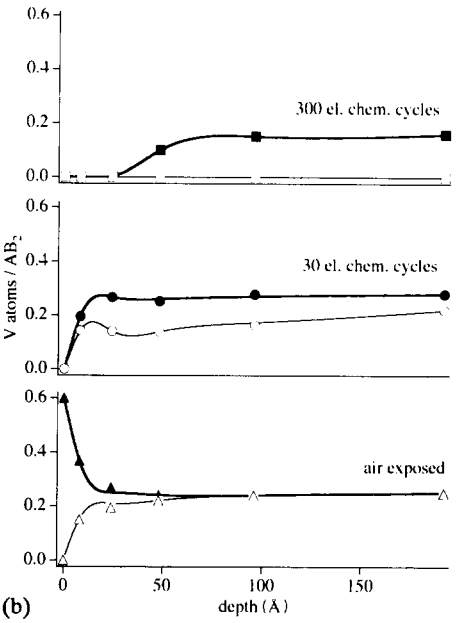

Fig. 8. XPS depth profiles of (a) Zr, (b) V and (c) Ni for $ZrV_{0.4}Ni_{1.6}$ at various stages of the cycle life curve (after a few hydrogen gas cycles, after 30 electrochemical cycles and after 300 electrochemical cycles). Solid data points represent the total amounts of the elements (metallic and oxidized states); open data points represent the metallic constituents of the elements in terms of atoms/AB_2 (where AB_2 stands for the sum Zr + V + Ni).

diffusion of OH^- ions into the double layer at the grain surface and diffusion of absorbed hydrogen to the surface of the grains, (2) adsorption of the OH^- ions on the adsorbed hydrogen, (3) charge transfer from the adsorbed $H\cdots OH^-$ complex to the metal, (4) desorption of the water molecule and finally (5) diffusion of the water molecule out of the double layer into the "bulk" electrolyte. Each step may be the rate-limiting step. In the gas phase it is known that for small samples heat and mass transport are minimal and therefore not regulating steps. However, there is a further step called nucleation and growth which can be a rate-controlling step [10]. In our experiments the capacity quotas as a function of the vanadium content correlated with the maximum measured discharge capacities. Assuming that the charge transfer is the rate-determining step, the exchange current would then be a measure of the kinetics of the charge–discharge reactions.

We observed similar characteristics of the exchange current *vs.* the vanadium content of the alloy. The curve, however, has a sharper maximum for the nickel than for the copper matrix electrodes.

The activation and degradation of the alloy with increasing cycles appear to be strongly influenced by the matrix material (copper or nickel). There are two possible explanations for this. One is that nickel has a heat conduction constant about five times smaller

than that of copper. The other explanation is that nickel is known as an electrochemically active material. During electrode preparation heat-shrunk tubing is used to fix the pellet to its holder. As a consequence, the pellet itself is heated to about 140 °C. Certain metals are susceptible to oxidation when heated. This oxidation decreases the activity of the alloy. On the other hand, nickel is more sensitive to oxidation and corrosion during cycling than copper. This raises the risk of losing grain-to-grain electrical contacts. Nickel matrix electrodes demonstrate a much higher activation constant than copper matrix electrodes but at the same time have a higher oxidation constant. The potential after charging and after discharging (open circuit) indicates the amount of hydrogen remaining in the alloy. The potential after charging reaches a maximum within the first 5 cycles and then remains constant. This indicates that the electrode is fully charged after a few cycles. The potential after discharging decreases slowly, with the exception of discharging at low currents. After 40 or more cycles it reaches a minimum and then begins to increase again. This indicates that an increasing amount of hydrogen remains in the alloy. We have concluded that higher electrical grain-to-grain resistance caused by the formation of nickel oxides is responsible for this increase in potential. Therefore degradation of the cycle life curve is not only due to corrosion of the alloy and the loss of potential hydrogen storage sites, but also to higher overpotentials resulting from worse grain-to-grain electrical contacts.

The XPS depth profiles of the alloy elements have shown that the main change in the alloy surface during activation is the dissolution of vanadium oxides and an enrichment of nickel in the near-surface layers. Nickel is a good catalyst for hydrogen dissociation and recombination, so we would assume that nickel also aids in the dissociation of water molecules and the recombination of hydrogen with hydroxyl ions. Both processes contain the same reaction steps, *i.e.* transfer of an electron from the metal to the hydrogen and adsorption of hydrogen on the metal. The depth profile of a degraded electrode indicates that the alloy corrodes during cycling by oxidation of the less noble elements and dissolution of their oxides.

5. Conclusions

An electrochemical analysis of a series of $Zr(V_xNi_{1-x})_2$ ($0 \leqslant x \leqslant 0.4$) alloys has demonstrated that $ZrV_{0.5}Ni_{1.5}$ is the alloy which has the highest hydrogen storage capacity and the best kinetics. Nickel proved to be a poorer electrode matrix material than copper because of its poor oxidation stability in the potential range used for these experiments. However, electrodes compacted with nickel powder indicated that heat treatment during fabrication may be the cause of activation problems with the alloys studied.

Finally, we have observed that several processes are involved in the degradation of the cycle life curve, namely loss of grain-to-grain electrical contact by oxidation, loss of hydrogen storage sites due to corrosion of the alloy, and dissolution of components of the less noble elements at the surface of the alloy.

Acknowledgment

Financial support for this research was received from the Bundesamt für Energiewirtschaft BEW (Swiss Department of Energy).

References

1 V.V. Petkov, V.Ya. Markiv and V.V. Gorskiy, *Russ. Metall. (Engl. Transl.), (2)* (1972) 137.
2 H. Sawa and S. Wakao, *Mater. Trans., JIM, 31* (6) (1990) 487.
3 S. Wakao and H. Sawa, *J. Less-Common. Met., 172–174* (1991) 1216.
4 S. Wakao, H. Sawa, H. Nakano, S. Chubachi and M. Abe, *J. Less-Common. Met., 131* (1987) 311.
5 H. Sawa, M. Ohta, H. Nakano and S. Wakao, *Z. Phys. Chem. N.F., 164* (1989) 1527.
6 F. Jaggy, W. Kieninger and R. Kirchheim, *Z. Phys. Chem. N.F., 163* (1989) 431.
7 A. Züttel, F. Meli and L. Schlapbach, *Z. Phys. Chem. N.F.*, in press.
8 A. Züttel, F. Meli and L. Schlapbach, *J. Alloys Comp., 200* (1993) 157.
9 Z.-P. Li, Y.-Q. Lei, C.-P. Chen, J. Wu and Q.-D. Wang, *J. Less-Common. Met., 172–174* (1991) 1260.
10 N. Gerard and S. Ono, Hydride formation and decomposition kinetics, in L. Schlapbach (ed.), *Topics in Applied Physics*, Vol. 67, *Hydrogen in Intermetallic Compounds II*, Springer, New York, 1992, Chap. 4, p. 166.